On the applicability of cold acoustic measurements to high-amplitude hot pulsating flows

Submitted to *Acoustics Australia*

A. J. Torregrosa, P. Piqueras, E. J. Sanchis and Á. Redondo

CMT-Motores Térmicos, Universitat Politècnica de València, Camino de Vera s/n, 46022 Valencia, Spain.

Abstract. The experimental characterization of the acoustic characteristics of engine exhaust devices is usually carried out through measurements in cold conditions, due to the intrinsic difficulties associated with proper temperature control in an acoustic rig. While those measurements may be sufficiently indicative for the cold end of the exhaust (the silencing elements) their significance for the hot end (the aftertreatment system) is more doubtful, as a result of the high temperatures and, eventually, the higher amplitude of pressure waves acting on the system. In this paper, a direct assessment is provided on the significance of acoustic measurements in cold conditions for representing the actual behaviour of an aftertreatment system in a hot pulsating, engine-like flow. Making use of wave decomposition techniques, the measured characterization was convoluted with the hot-flow excitation and the device responses were directly compared. The results indicate that, while it is not possible to fully reproduce the behaviour observed in hot pulsating flow, the tendencies are reproduced, at least qualitatively. In particular, the effect of soot loading is fairly reproduced.

Keywords: acoustics, experimental characterization, pulsating flow, aftertreatment system, temperature, wave decomposition

1. Introduction

Current energy policies worldwide exhibit an evident concern for air quality that has led to the approval of regulations that limit pollutant emissions from internal combustion engines [1]. These regulations apply to spark ignition (SI) [2] and compression ignition (CI) engines [3]. The increasingly restrictive nature of these regulations has led to the technological solution revolving around the necessary implementation of exhaust aftertreatment systems (ATS) to eliminate pollutant species before they are emitted into the atmosphere [4].

Among the ATS, various systems are composed of catalysts impregnated on flow-through monoliths. This type of ATS makes it possible to eliminate gaseous emissions produced during combustion, such as NOx, HC, and CO, and some secondary gaseous emissions. Otherwise, for

the elimination of particulate material (PM), particulate filters (PF) [5] are commonly used, both in CI engines [6] and Direct Injection SI (DI-SI) engines [7]. In both cases, PF can also be impregnated with catalyst, either to facilitate its regeneration or to provide it with the function of removing gaseous pollutants [8].

The ATS layout in the exhaust line is usually conditioned by the ideal operating temperatures and the possible interactions between the different ATS. This is the case of the diesel oxidation catalysts (DOC) and the diesel particulate filter (DPF), which are usually placed together in a single canning [6]. This is done because the most common regeneration method is late fuel post-injections, which involves injecting a quantity of fuel in single or separate portions after the main injection during the expansion stroke [9]. The extra fuel injection results in a significant increase in the concentration of HC in the exhaust gases, which is burned in the DOC with a consequent increase in gas temperature [10] that promotes DPF regeneration.

The presence of these dissipative systems upstream of the muffler modifies the boundary conditions for its design, which usually leads to a substantial reduction in volume or even its elimination [11]. For this reason, the determination of the acoustic effects of the ATS is essential to guarantee the correct design of this element [12]. Acoustic modelling tools are of fundamental help for this task, covering a broad spectrum of solution approaches. The first attempts to model unsteady flow in catalytic honeycomb structures were restricted to the linear regime and date back to the work of Glav et al. [13]. Currently, among these tools one can find those based on linear and nonlinear methods, with different levels of spatial resolution, from the most complex and computationally expensive, with a 3D approach [14], to simple models based on phenomenological solutions [15], going through those with an intermediate complexity such as quasi-3D cells models [16] and 1D/2D models [17]. There is also variety in the numerical schemes used, comprising models that use finite element methods (FEM) [18] for the analysis of wave propagation along monolith channels, and boundary element methods (BEM) to account for 3D effects in the inlet and outlet canning volumes [12]. Otherwise, PF modelling requires specific tools capable of predicting its operation under different unsteady flow conditions and with different PM loading. Among the first PF models is the one presented by Allam and Abom, based on a linear 1D solution [19]. This model is the basis for the definition of the transfer matrix in other more complex linear models, based on 3D-FEM solutions that provide a better prediction of the PF response at high frequencies [20]. While all these theoretical tools are fundamental to the analysis and optimization of the acoustic response of ATS, their validity is highly dependent on the availability of reliable experimental data. In the literature, there is a wide variety of techniques

for measuring the acoustic behaviour of dissipative systems [21]. These techniques range from techniques with external sound level meters [22] to techniques using multiple sensors in the ducts [23]. In this last approach, it is possible to find methods with different degrees of complexity, from those that use two sensors located at the inlet and outlet of the element to be analysed [24], to those that use multiple sensors at the inlet and outlet and allow systems to be characterized with greater complexity, both at the structural level and regarding flow conditions [21].

Due to the intrinsic difficulties involved in controlling the temperature during the measurements, all these techniques are usually applied at room temperature, and thus they provide validation criteria for the models at such temperature conditions. While this does not pose any significant problem in the case of the silencers, that operate at moderately high temperatures, in the case of the aftertreatment systems, that operate at the highest temperatures in the exhaust line, some doubts may arise. In fact, it was recently proven that, in the case of aftertreatment systems, the pressure drop does not follow in full the expected similarity as a function of the Reynolds number, and the differences could not be explained on the single basis of compressibility effects [25]. Therefore, it is interesting to dispose of some assessment of the actual performance of extrapolating the results of acoustic measurements at room temperature to hot-flow conditions. The purpose of this work is to provide such an assessment.

The paper is organized as follows. First, the ATS used is described, the measurement set-ups and procedures used to characterize its acoustic behaviour at room temperature and to gather data on its behaviour under hot pulsating flow conditions are reviewed and discussed. Then, the assessment procedure devised is explained, together with all the required post-processing of the raw experimental data. This is followed by the discussion of the results obtained. Finally, the main conclusions of the work are summarized.

2. Materials and methods

The ATS considered consisted of a DOC and a DPF in the same canning, and its main characteristics are listed in table 1. In order to collect the experimental information required for the assessment sought, two experimental facilities were used. The first, the impulse test rig, allows tests to be carried out using an isolated pressure pulse either with or without a superimposed mean flow. The second installation, the unsteady flow gas stand, was used to carry out tests with engine-like, unsteady periodic flow under controlled temperature and mass flow conditions. Tests were carried out both with the ATS in clean conditions and in soot-

loaded conditions. The soot loading process was conducted on a commercial high-speed, direct-injection CI engine, until the DPF reached loading conditions of 13 g/l of soot. By carrying out the tests with the ATS in clean and in soot-loaded conditions, it was possible to account for the influence that the soot load has on the acoustic behaviour of the system.

Table 1. Main DOC and DPF geometric parameters.

	DOC	DPF
Monolith diameter [mm]	172	172
Monolith length [mm]	82	105
Channel cross-section	Square	Square
Cell density [cpsi]	400	200
Cell size [mm]	1.17	1.40
Wall thickness [mm]	0.101	0.40
Catalytic area [m^2]	5.52	–
Filtration area [m^2]	–	2.11

2.1. Impulse test rig

First, the acoustic characterization of the ATS was conducted in the impulse test bench, whose design is based on an improved version of the impulse method [26]. This installation allows the acoustic response of an ATS to be analysed by subjecting it to an isolated pressure pulse of controlled amplitude and duration. The reflected and transmitted pressure pulses generated as a result of the incidence of the pressure pulse on the ATS are recorded by piezoelectric pressure sensors. Figure 1 shows the scheme of the experimental setup and its operating principle.

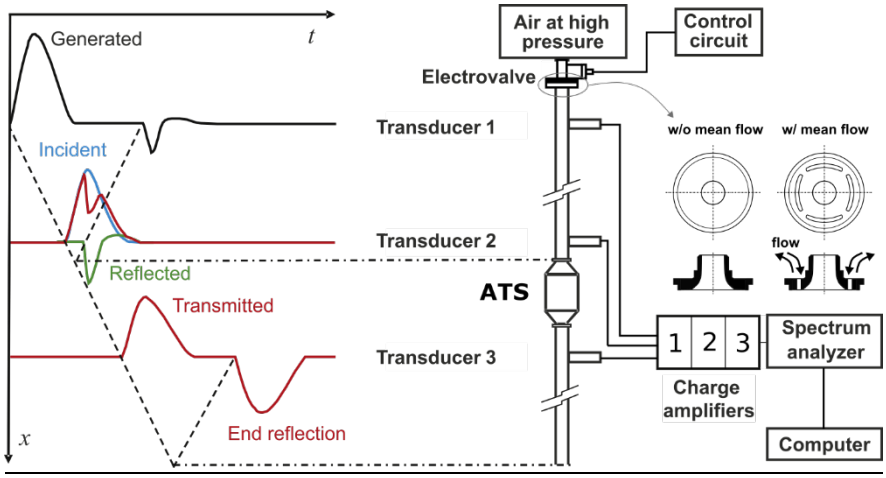

Figure 1. Schematic setup of the impulse test rig.

The impulse method is based on generating a pressure pulse at room temperature by the successive opening and closing with a high-speed electrovalve of the flow path from a pressurized tank. The duration of the opening period controls the duration of the generated pulse and, together with the tank pressure, the generated pulse amplitude is also controlled.

In this installation, it is possible to carry out characterization tests with and without a superimposed mean flow. This aspect of the test is controlled by the nozzle used at the outlet of the electrovalve. As shown in figure 1, the use of a perforated nozzle allows for superimposed mean flow, whereas a non-perforated nozzle avoids it. The mass flow in the tests with superimposed mean flow is controlled by acting on the pressure of the tank, what may imply limitations to the amplitude of the pulses generated.

Regarding the operation of the installation, the generated pulse is measured by transducer 1, which is located in the duct that connects the outlet of the electrovalve with the ATS, through which the pulse propagates. The length of this duct and the position of transducer 1 are selected so that the correct development of the pulse is allowed for, while ensuring that the measurement of transducer 1 is not affected by the reflected pulse traveling in the opposite direction from the ATS towards the electrovalve. The location of this transducer and the recorded pressure are shown in figure 1.

Transducer 2 is located right at the inlet of the ATS, and the superposition of the incident and reflected pulses (p_{comp}) is measured there. In order to identify the incident and reflected pulses, the following procedure is carried out as described in [26]:

i. The ATS is tested with multiple generated pressure pulses with the same amplitude and duration (repeatability within a prescribed uncertainty below 5%). These tests provide the profiles of the generated pressure pulse, the superposition of the incident and reflected pulses in the ATS inlet section and the transmitted pressure pulse in the outlet section.
ii. The ATS is replaced with a straight duct and the test is repeated using generated pressure pulses similar to those used in step 1. In this way, the pressure pulse recorded in transducer 1 is similar to the incident pulse that excites the ATS in step 1. These tests provide the profiles of the generated and incident pressure pulses.
iii. The best matching pair of step 1 and step 2 tests are identified based on the comparison of the generated pressure pulses recorded by transducer 1, using the statistical procedure described in [15]. Once the matching tests are selected, the incident pressure pulse in the ATS test (step 1) is considered equal to that measured by transducer 2 in the straight duct

test (step 2). This incident pressure pulse is combined with the measurement of transducer 2 in the ATS test to determine the reflected pressure pulse applying equation (1) [27],

$$\left(\frac{p_{ref}}{p_0}\right)^{\frac{\gamma-1}{2\gamma}} = \left(\frac{p_{comp}}{p_0}\right)^{\frac{\gamma-1}{2\gamma}} - \left(\frac{p_{inc}}{p_0}\right)^{\frac{\gamma-1}{2\gamma}} + 1 \quad (1)$$

where γ is ratio of specific heats and p_0 represents the pressure of the unperturbed medium.

Finally, the pressure pulse transmitted downstream of the ATS is registered by transducer 3, that is located close to the outlet of the ATS, and an outlet duct of a suitable length is used to avoid that the measurement registered is affected by secondary reflections from the open end.

This process makes it possible to obtain the coefficients of the ATS scattering matrix in an excitation direction, either in or against the direction of flow propagation when the ATS is installed in the engine. For the complete acoustic characterization of the ATS, it is necessary to determine the response in both directions of excitation. This can be done experimentally when the ATS is in clean condition by repeating each test twice:

- In the direct test, the ATS is excited at the inlet, so that the inlet reflection coefficient r_1 and the inlet-to-outlet transmission coefficient t_{12} can be determined.
- In the reverse test, the ATS is excited at the outlet, and thus the reflection coefficient at the outlet r_2 and the transmission coefficient from the outlet to the inlet t_{21} can be evaluated.

Since the direction of propagation of the pulse in the installation cannot be changed, the change from direct test to reverse is done by reversing the ATS position in the impulse test rig.

In the case of ATS in soot load conditions, it is impossible to carry out the reverse test without causing the detachment of the layer of soot. For this reason, the methodology described in [28] was used, which allows estimating the inverse response of the system based on the reciprocity properties and the dissipation of the ATS.

The methodology described was carried out in such a way that the test protocol listed in Table 2 was completed for the ATS both in clean condition and in soot-loaded condition. Tests without superimposed mean flow were carried out with three pulses with different amplitudes, and with superimposed mean flow a single pulse amplitude was considered.

Table 2. Amplitude and duration of the incident pulse generated in the impulse test rig and values of the superimposed mean flow

		Duration [ms]	
		11	14
Amplitude [mbar]	80	w/o mean flow	-
	150	-	w/o mean flow
	150	-	mean flow 170 kg/h

The raw results from the measurements are shown in the time domain in figure 2(a), where it can be observed that they are consistent with what should be expected: an increase in the pulse amplitude produces an increase in the pulse propagation velocity so that pulses with a higher amplitude arrive before at the measurement stations. This advance is more apparent in the case with superimposed mean flow, where the effect of the flow on the mean pressure can also be clearly observed. The results in the frequency domain are shown in figure 2(b), where it can be seen that the pulses used are able to excite all the frequencies of interest, but they exhibit a certain ripple that will be commented later on when referring to the determination of the scattering matrix elements.

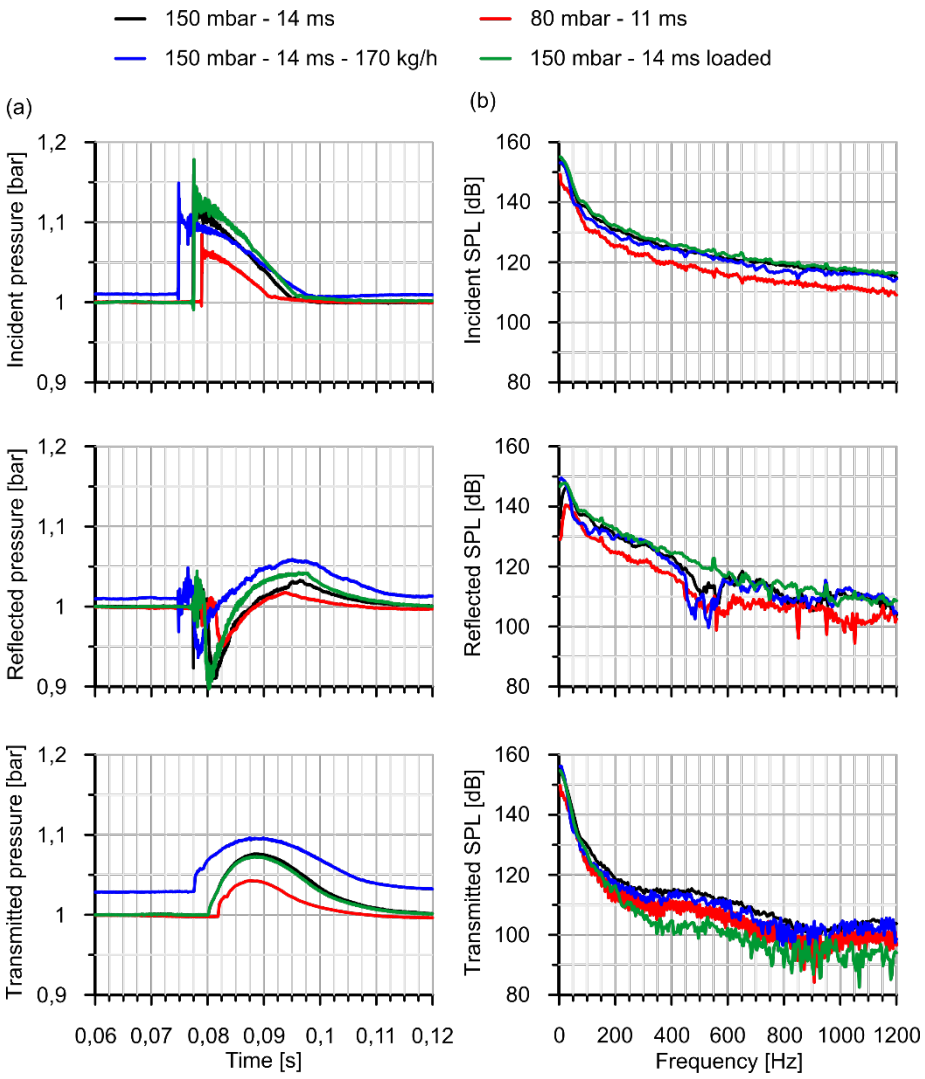

Figure 2. Impulse rig: raw results: (a) time domain; (b) frequency domain.

2.2. Unsteady flow gas stand

The schematic configuration of the unsteady flow gas stand used is shown in figure 3: the air is pumped from the atmosphere by means of a screw compressor whose rotational speed determines the mass flow. Downstream of the compressor, the flow is heated by a set of electric heaters. The flow is then conveyed to a rotary valve with a bypass system, thus generating the pulsating flow. The amplitude and frequency of the pulses are controlled by the opening of the bypass valve and the speed of the rotary valve, respectively.

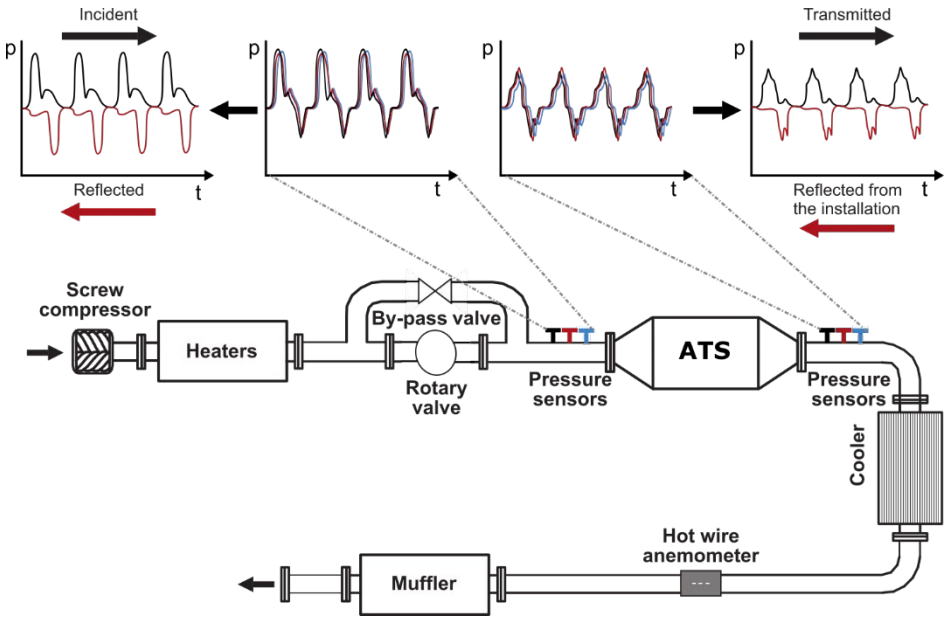

Figure 3. Setup of the flow gas stand.

The instrumentation used in these tests include different sensors to control the gas stand and to characterize the operating conditions of the ATS. The flow temperature was measured with four thermocouples located in cross-sections at 0.9 m from the inlet and outlet of the ATS. The mass flow was controlled with a hot-film anemometer located downstream of a heat exchanger that was located close to the tailpipe of the gas stand. The absolute mean pressure was measured using Kistler 4045A5 cooled piezoresistive sensors installed upstream and downstream of the ATS. Finally, for the instantaneous measurement of pressure, six Kistler 7061B cooled piezoelectric transducers were used, coupled to Kistler 5011B load amplifiers. The main characteristic of this set is their high sensitivity, which allows the detection of pressure fluctuations below 200 Pa. These transducers were placed in two groups of three at the inlet and the outlet of the ATS at equally spaced axial positions, this particular disposition allowing for the estimation of wave components through post-processing.

From the information collected in these tests, the wave components in both propagation directions at the inlet and the outlet of the ATS were estimated by means of the application of a beamforming technique [29], as shown schematically in figure 3. In this way, it is possible to evaluate the sound pressure level reflected and transmitted by the ATS. The beamforming technique used assumes that the pulse propagation between sensors is linear, which is acceptable if the array aperture (total length) is small when compared with the wavelength.

An extensive experimental plan was carried out, from which a reduced sample of six operating points allowing for back-to-back comparison of the influence of the different relevant

parameters (mass flow, temperature, pressure amplitude and frequency, and loading) is shown here. These operating conditions are shown in table 3, where the parameters diff from those of the baseline are highlighted in bold type. The pulse frequencies were selected based on frequencies close to those associated with different engine speeds, e.g., 100 Hz is equivalent to the operation of a four-cylinder engine running at 3000 rpm. The effect of soot loading was analysed at 200 ˚C in order to avoid regeneration in the presence of O_2 [30].

Table 3. Operating points: mass flow, temperature and pulse characteristics.

Frequency [Hz]	Mass flow [kg/h]	Temperature [◦C]	Amplitude [bar]	Loading
33	300	200	0.25	no
33	300	200	**0.10**	no
100	300	200	0.25	no
33	300	200	0.25	**yes**
33	300	**500**	0.25	no
33	**500**	200	0.25	no

An example of the raw results obtained is shown in figure 4. It is apparent, in view of the small differences existing between the signal recorded by the three transducers in the array, that a careful calibration is imperative, both in amplitude and phase. The details of the calibration procedure can be found in [29].

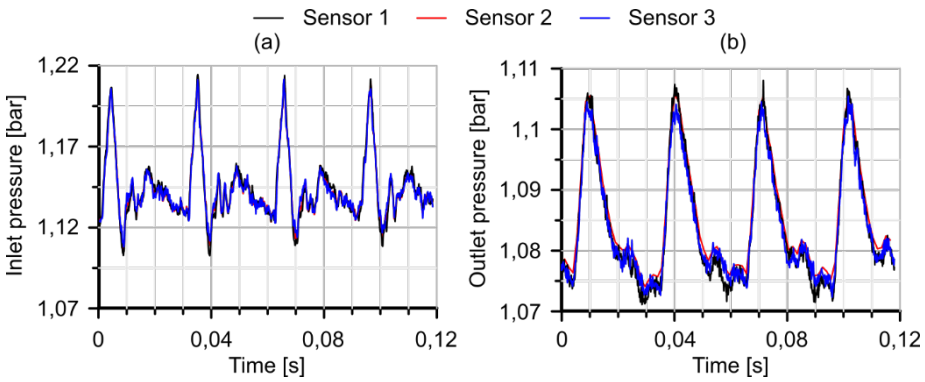

Figure 4. Example of raw measurements in the unsteady flow gas stand ($f = 33$ Hz, $\dot{m} = 300$ kg/h, $T = 200$ ℃, $\Delta p = 0.1$ bar, clean): (a) upstream; (b) downstream.

3. Assessment procedure

The procedure used for the assessment is essentially an experimental implementation of the time-frequency computational method described in [31]. Consider the situation depicted in figure 5, where the ATS together with the upstream and downstream pressure components have been represented.

Figure 5. Nomenclature for pressure components.

Interpreting this in terms of excitation (pressure components traveling towards the system, p_1^+ and p_2^-) and response (pressure components traveling away from the system, p_1^- and p_2^+), and assuming linear propagation across the device, the forward and backward pressure components upstream and downstream will be related by the scattering matrix, as

$$\begin{pmatrix} p_2^+ \\ p_1^- \end{pmatrix} = \begin{pmatrix} t_{12} & r_2 \\ r_1 & t_{21} \end{pmatrix} \begin{pmatrix} p_1^+ \\ p_2^- \end{pmatrix} \tag{2}$$

The relation expressed in (2) provides the natural way of extrapolating the characterization given by the scattering matrix to flow conditions different from those in which it was measured. For its application to the hot pulsating flow of the gas stand, the pressure components were obtained from the beamforming decomposition outlined in section 2.2, providing both the input for equation (2) and the response components to be compared with the output of equation (2), thus allowing for the assessment of the extrapolation of the scattering matrix to engine-like conditions. With respect to the elements of the scattering matrix themselves, they are available at room temperature from the measurements summarized in section 2.1; they must however be corrected for the flow and the temperature existing in the hot gas stand.

The influence of flow conditions at room temperature was analysed in detail in [15], where a suitable parameterization of the elements of the transmission matrix in terms of two Fourier series was introduced. If $\psi_b(f)$ denotes the real or the imaginary part of any element of the scattering matrix obtained experimentally for the baseline operating point (b), it can be expressed as the sum of two terms as

$$\psi_b(f) = \varphi_b(f) + \varepsilon_b(f) \tag{3}$$

The first term, $\varphi_b(f)$, is the Fourier series fitted for the baseline operating point:

$$\varphi_b(f) = \sum_{k=0}^{n} \left[a_k \cos\left(k\tau_{b,exp} f\right) + b_k \sin\left(k\tau_{b,exp} f\right) \right] \quad (4)$$

where a_k and b_k are the Fourier series constants, and $\tau_{b,exp}$ is the characteristic period. The second term is the Fourier series fitted to the difference between the result of applying equation (4) and the actual experimental data:

$$\varepsilon_b(f) = \sum_{k=0}^{n} \left[a'_k \cos\left(k\tau'_{b,exp} f\right) + b'_k \sin\left(k\tau'_{b,exp} f\right) \right] \quad (5)$$

The advantage of this procedure is its robustness to reproduce the shift that the elements of the scattering matrix suffer when the propagation velocity varies. Firstly, it was found that function $\varepsilon_b(f)$ is the same for any device and any element of the scattering matrix. Regarding function $\varphi_b(f)$, it was found that the constants of the Fourier series are representative of the geometry, whereas the characteristic period is sensitive to any kind of excitation variation that produces a change in propagation velocity, and thus it is the only parameter that must be modified in order to capture the shift. This actually allows for using only the scattering matrix measured for a certain baseline flow condition, if one is able to figure out how to modify τ_b.

The required change in the characteristic period was estimated as that required in order to reproduce the change experienced by the elements of the scattering matrix of a simple straight duct when temperature and mean mass flow are modified, as these elements are explicit functions of the two dimensionless quantities characterizing the physics of wave propagation: the Helmholtz number, $\mathrm{He} = kl$, where k is the wave number and l is the duct length, and the Mach number, Ma.

As an additional benefit of this procedure, any small inconsistencies in the experimental results, mainly due to the need to combine the results of direct and inverse tests, are conveniently smoothed out, thus providing a convenient representation allowing for a sound interpolation of the data at frequencies different from those directly available in the measurements. The resulting modulus of the elements of the scattering matrix can be seen in figure 6, being apparent that the procedure provides conveniently smoothed, suitable for interpolation, results, whereas the measured raw spectra shown in figure 2 exhibited a much more oscillating behaviour.

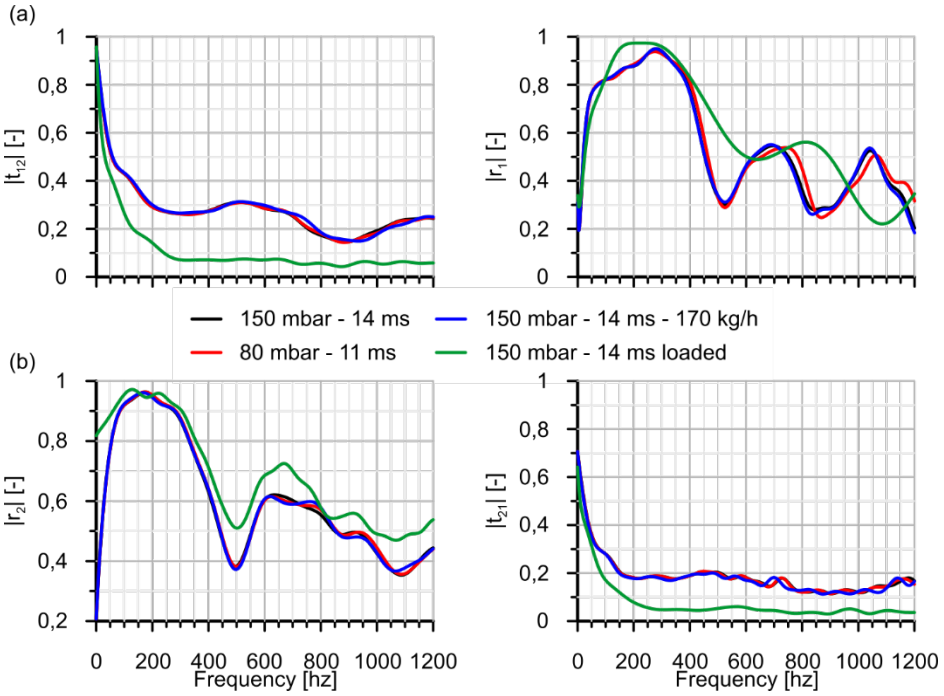

Figure 6. Impulse rig: transmission and reflection coefficients: (a) direct; (b) inverse.

Additionally, it can be observed that neither the mean flow nor the pulse amplitude have a strong influence on the acoustics of the device, at least for the range tested, and the influence observed is that expected. On the contrary, the loading of the device has a significant impact on the transmission coefficients, whereas the effect on the reflection coefficients is less pronounced but still important. Regarding the influence of temperature, the same procedure was used for the extrapolation of the measured scattering matrix, as changes in temperature affect the coefficients also through the Helmholtz and the Mach numbers.

Regarding the input (p+ and p−) to (2) and the output to be compared with the results of applying (2), the results of the decomposition procedure corresponding to the raw measurements shown in figure 4 are shown as an example in figure 7 (mean values are not provided by the decomposition procedure and they have been assigned arbitrarily to provide the best view of the time domain curves). It can be observed that the wave components upstream of the ATS exhibit larger amplitudes than the downstream components, as expected.

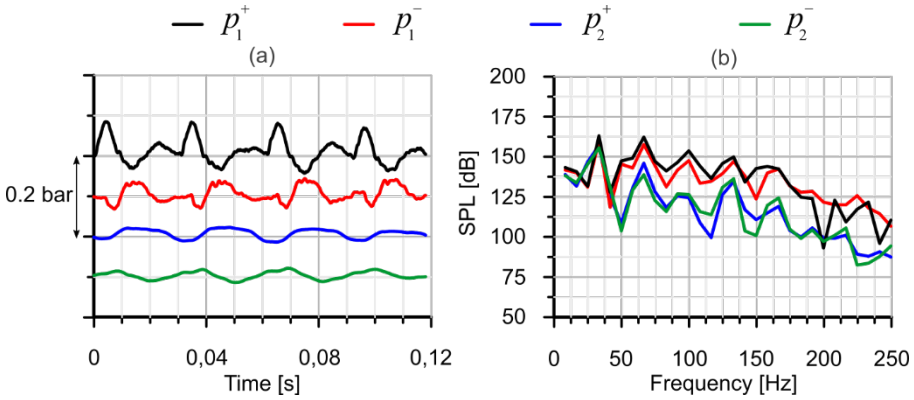

Figure 7. Example of wave decomposition results ($f = 33$ Hz, $\dot{m} = 300$ kg/h, $T = 200$ ℃, $\Delta p = 0.1$ bar, clean): (a) upstream; (b) downstream.

4. Results and discussion

The results obtained from the application of the assessment procedure are presented in figures 8 and 9, for the first eight engine orders (H2 to H16) of the equivalent four- cylinder, four-stroke engine. This is well beyond the usual range of interest in exhaust applications, where the relevant range rarely exceeds the fourth engine order [32]. As commented above, what is being compared here is the output components p_1^- and p_2^+ identified by the wave decomposition procedure (labelled as “wave decomposition”) and those obtained from the application of equation (2) (labelled as “scattering matrix”).

Regarding the upstream backward components, it can be seen in figure 8 that, overall, there is an acceptable agreement between the levels estimated through the extrapolated scattering matrix and those directly obtained from wave decomposition. Considering the baseline configuration, figure 8(a), it is apparent that the tendency of the sound pressure level is perfectly reproduced, while discrepancies in the actual level are within 5 dB, that is in the order that is considered acceptable for model validation in industrial practice. In this case, additionally, the values provided by the scattering matrix lie above those obtained from wave decomposition, except in the first order, where the difference is very small.

When the pressure amplitude is decreased down to 0.1 bar, see figure 8(b), the results still follow the general evolution, even if the behaviour in more erratic. This might be reasonable considering that, consistently with the comments to figure 4, for such small amplitudes the noise-to-signal ratio of the measurements poses serious challenges to the use of wave decomposition, even if a robust algorithm is used.

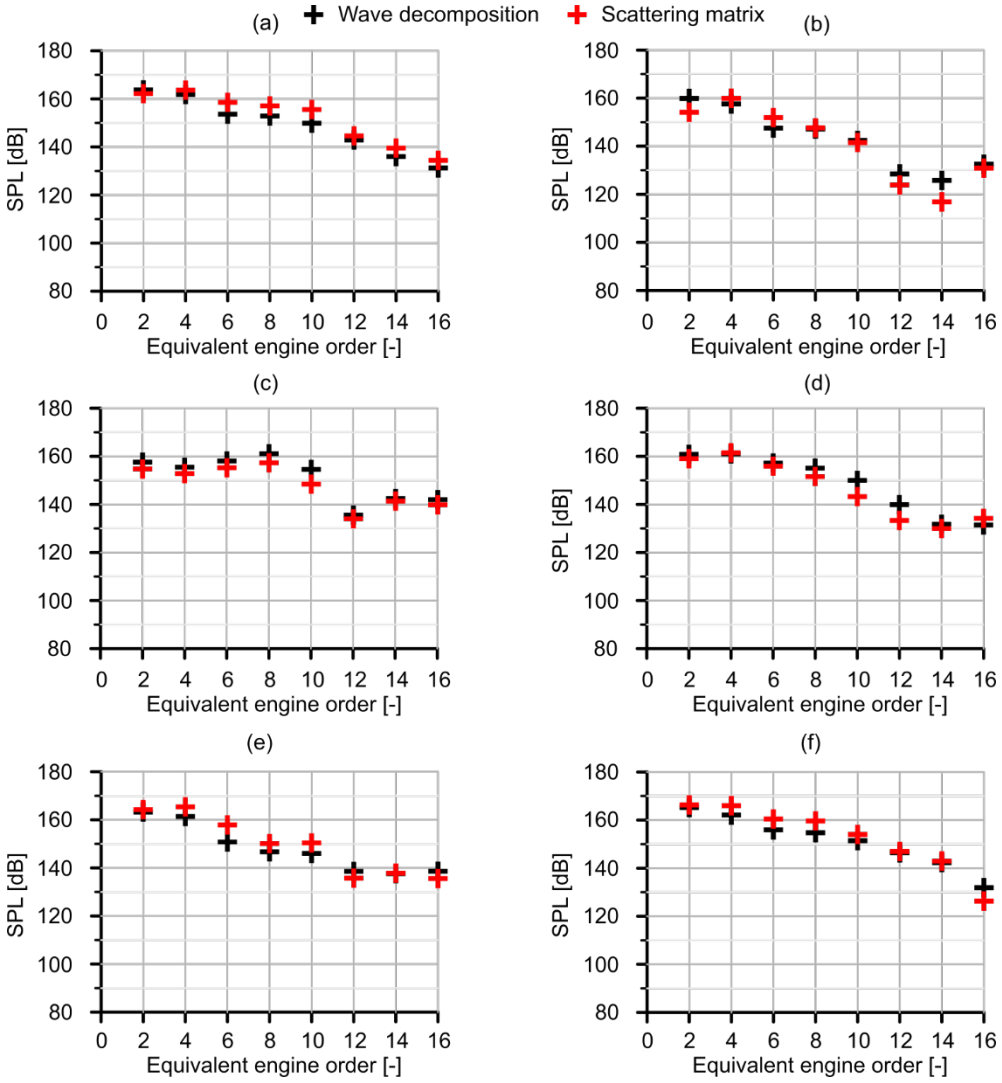

Figure 8. Comparison of measured and estimated backward components upstream of the ATS, p_1^-: (a) baseline ($f = 33$ Hz, $\dot{m} = 300$ kg/h, $T = 200$ ℃, $\Delta p = 0.25$ bar, clean); (b) $\Delta p = 0.1$ bar; (c) $f = 100$ Hz; (d) loaded; (e) $T = 500$ ℃; (f) $\dot{m} = 500$ kg/h.

The change in the frequency does not introduce any new features, as it is observed in figure 8(c). The maximum deviation is of the order of that of the baseline point, but the trend is followed even better than for those conditions. The same comments apply to the effect of soot loading, shown in figure 8(d): again, the maximum deviation is comparable, and the evolution of frequency is fairly captured. With respect to the effect of increasing the temperature or the mass flow, one may observe in figures 8(e) and 8(f) that the results are of a similar quality when compared with the baseline case, with the exception of the sixth order of the temperature variation, in which the highest deviation for any of the conditions tested is observed, even though the dependency with the order number is well reproduced. As a conclusion, it appears that the extrapolated scattering matrix is able to provide a sufficiently representative picture of the effects of the ATS on the flow upstream of the device.

The corresponding comparison for the downstream forward components is shown in figure 9 where, again, a fair reproduction of the results provided by wave decomposition can be observed overall, although the quality of the results is slightly worse than for the upstream backward components. Accordingly with previous comments, this might be expectable, since the ATS produces a significant decrease in amplitude and thus any negative repercussions of the noise-to-signal ratio on the performance of the wave decomposition method should be more apparent.

In any case, deviations lie within the same order as in the case of the upstream backward components, with some exceptions that, in all the cases but one (see figure 9(f)), correspond to orders above the tenth, thus being associated with relatively low amplitudes and out of the usual range of interest. The same applies to the reproduction of the trend with respect to the engine order: any failures to reproduce it lie in the same orders as for the significant amplitude deviations. The only exception in both cases is the operating point corresponding to a mass flow of 500 kg/h shown in figure 9(f). A reasonable explanation would come here again from the consideration of the noise-to-signal ratio of the measurements: the high velocities occurring in this operating condition should give rise to strong turbulent fluctuations that, in the upstream side, can be overcome by the relatively high amplitude of the deterministic signal but, in the downstream side, may be an insurmountable difficulty for the decomposition algorithm.

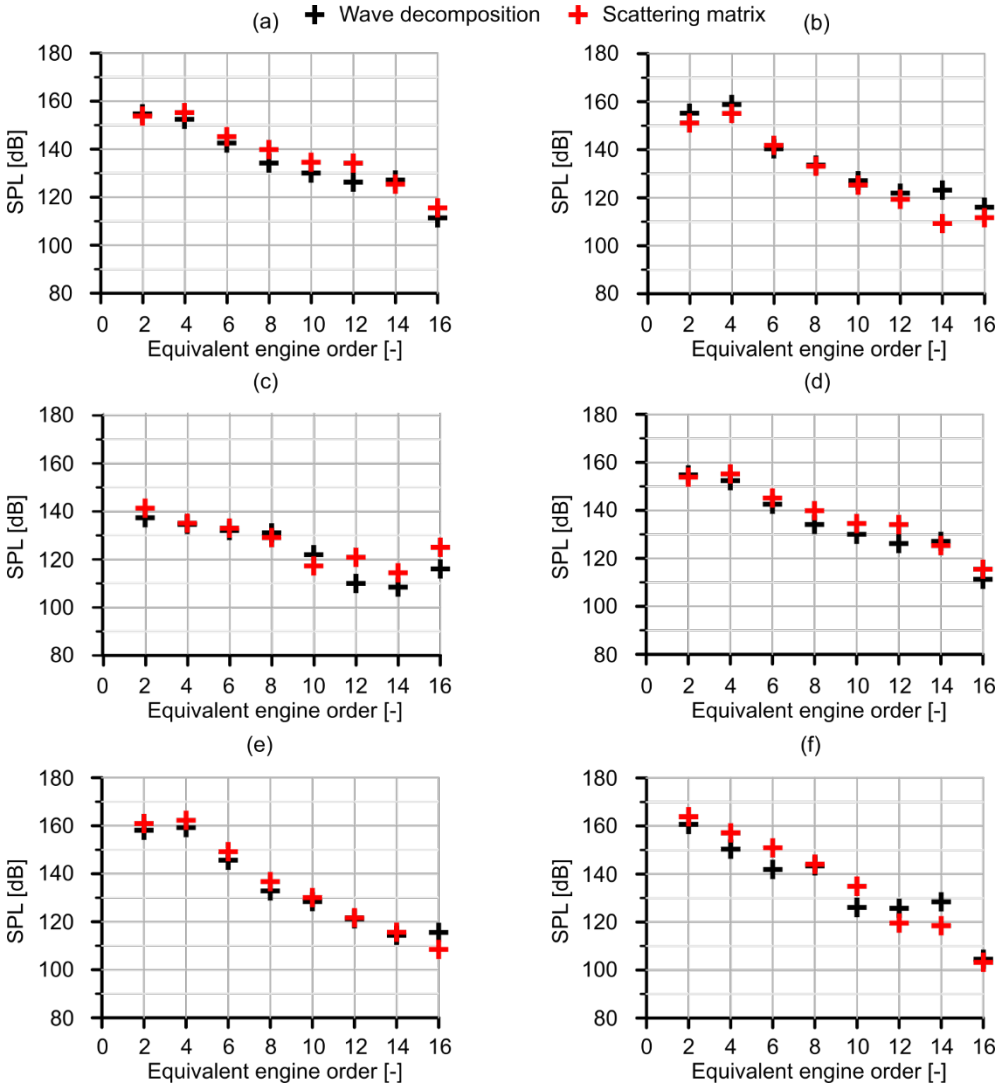

Figure 9. Comparison of measured and estimated backward components upstream of the ATS, p_2^+: (a) baseline ($f = 33$ Hz, $\dot{m} = 300$ kg/h, $T = 200$ °C, $\Delta p = 0.25$ bar, clean); (b) $\Delta p = 0.1$ bar; (c) $f = 100$ Hz; (d) loaded; (e) $T = 500$ °C; (f) $\dot{m} = 500$ kg/h.

5. Summary and conclusions

The significance of acoustic measurements taken under cold laboratory conditions with regards to actual engine operating conditions, i.e., with hot and pulsating flow, was assessed. For this purpose, an ATS containing a DOC and a DPF in a single shell was studied. Characterization in impulse test rig at cold condition provided the base terms of the scattering matrix at room conditions, just aside of additional corrections needed to compensate for the flow and temperature as required. Measurements in the unsteady flow gas stand provided values of forward and backward components through a beamforming wave decomposition procedure. From these measurements it was evidenced that the wave components upstream of the ATS exhibit larger amplitudes than downstream components, as expected. Later, direct

comparison was made between two sets of data, those extracted from the wave decomposition, and those obtained with the extrapolation based on the scattering matrix approach, as presented in equation (2). Details on both approaches were presented.

A first insight into the effects on the acoustic behaviour of the different variables considered was provided by the values of the transmission and reflection coefficients obtained from the impulse test rig measurements:

- Mean flow and pulse amplitude showed weak influence within the range tested, but their effect was as expected.
- Soot loading showed an important influence on both sets of coefficients, especially on the transmission coefficients.
- In the case of temperature, the whole procedure of extrapolation was applied as temperature changes are also reflected in the Helmholtz and the Mach numbers.

From the application of the wave decomposition technique a major difficulty arose in several cases, as it was evidenced that the noise-to-signal ratio of the measurements poses serious challenges to the use of the procedure, even when the algorithm has been thoroughly conditioned. For the direct assessment the case chosen as the baseline for the analysis corresponds to the clean device, under a mass flow rate of 300 kg/h, a temperature of 200 ◦C, a frequency of 33 Hz and a pressure amplitude of 0.25 bar. Changes were then considered in each of these conditions: soot loading, increased mass flow (500 kg/h), temperature (500 ◦C) and frequency (100 Hz), and a reduction in pressure amplitude (0.1 bar). Results were plotted for the first eight engine orders (H2 to H16) of the equivalent four cylinder, four-stroke engine, which is beyond the usual range of interest in exhaust applications. The analysis of results was focused on the upstream backward component and the downstream forward component; regarding the first one:

- There is an acceptable agreement between the results from the wave decomposition and the scattering matrix extrapolation for all the scenarios. Tendencies are clearly captured but with certain deviations in the precise values, most of the deviations found being within 5 dB which is considered acceptable for model validation in industrial practice.
- In the baseline case, extrapolation overestimates wave decomposition except in the first order, where the difference is very small.

- The decrease in pressure amplitude to 0.1 bar caused the most remarkable difference between the two sets of results, but once again the tendency was properly reproduced. This is thought to be linked to the noise-to-signal ratio.
- Soot loading, increased mass flow and increased frequency do not induce any significant changes in behaviour; in all these cases the trend is adequately captured, especially in the last case, with deviations of the same order as for the baseline case.
- Increased temperature presented in the sixth order the highest deviation for any of the cases, but besides this the trend and dependency with order number are well reproduced.

From the results of the corresponding comparison for the downstream forward component the following conclusions were drawn:

- Except for the increased mass flow, which requires its own analysis, a fair reproduction of the results and trends was obtained, although the quality of the results is slightly worse than for the upstream backward components. This can be explained by the passage through the ATS causing an amplitude decrease and worsening the noise-to-signal ratio.
- With a couple of exceptions, both occurring above the tenth order, all deviations are within the 5 dB reasonable margin.
- The reproduction of the trend with respect to the engine orders is in general satisfactory, with the discrepancies being either by a small margin at the lowest orders or punctual at orders out of the usual range of interest.
- The case of increased mass flow (500 kg/h instead of 200 kg/h) presented noticeable deviations for most of the orders, and the trend was not well captured either. Once again, the noise-to-signal ratio provides a reasonable explanation as the consequent higher flow velocities should cause strong turbulent fluctuation which can be overcome by the algorithm with the relatively high amplitude of the deterministic signal in the upstream side, but not in the downstream side.

Overall, the extrapolated scattering matrix was found capable of providing indicative and representative information, at least qualitatively, of the effects of the ATS on the flow upstream and downstream of the device for the hot pulsating condition, particularly upstream. In general, expected effects of each of the variables considered were fairly reproduced and identified, in particular those of soot loading, regardless of the effect being observed in the elements of the scattering matrix, the components drawn from the wave decomposition or the

application of the extrapolation with the scattering matrix. It may thus be concluded that, within unavoidable uncertainties related with engine-like operation, acoustic measurements taken at room temperature provide relevant information for exhaust system hot-end design in an industrial environment.

Funding

This research has been supported by Grant PID2020-114289RB-I00 funded by MCIN/AEI/10.13039/501100011033. Álvaro Redondo is supported by Universitat Politècnica de València through the Programa de Ayudas de Investigación y Desarrollo [PAID–01–19] which grants his predoctoral contract.

Declarations

Conflict of interest: The authors declare no conflict of interest.

References

1. Hooftman, N., Messagie, M., Van Mierlo, J. Coosemans, T.: A review of the European passenger car regulations – Real driving emissions vs local air quality. Renew. Sust. Energ. Rev. **86**, 1–21 (2018).
2. Paredi, D., Lucchini, T., D'Errico, G., Onorati, A., Pickett, L., Lacey, J.: CFD modeling of spray evolution for spark-ignition, direct injection engines. AIP Conf. Proc. 2191 020125 (2019).
3. Telli, G.D., Altafini, C.R., Costa, C.A., Rosa, J.S., Martins, M.E., Rocha, L.A.O.: A comprehensive review of homogeneous charge compression ignition (HCCI) engines: Advantages, challenges and evolution. SAE Technical Paper 2020-36-0042 (2021).
4. Pla, B., Piqueras, P., Bares, P., Aronis, A.: Simultaneous NOx and NH3 slip prediction in a SCR catalyst under real driving conditions including potential urea injection failures. Int. J. Engine Res. **23**(7), 1213-1225 (2022).
5. Bermúdez, V., Ruiz, S., Conde, B., Soto, L.: Analysis of the aftertreatment performance in HD-SI engine fueled with LPG. Int. J. Engine Res. in press. DOI 10.1177/14680874211048138.
6. Piqueras, P., Burke, R., Sanchis, E.J., Diesel, B.: Fuel efficiency optimisation based on boosting control of the particulate filter active regeneration at high driving altitude. Fuel **319**, 123734 (2022).
7. Piqueras, P., Sanchis, E.J., Herreros, J.M., Tsolakis, A.: Evaluating the oxidation kinetic parameters of gasoline direct injection soot from thermogravimetric analysis experiments. Chem. Eng. Sci. **234**, 116437 (2021).

8. Matarrese, R.: Catalytic materials for gasoline particulate filters soot oxidation. Catalysts **11**, 890 (2021).
9. Farhan, S.M., Wang, P.: Post-injection strategies for performance improvement and emissions reduction in DI diesel engines - A review. Fuel Process. Technol. **228**, 107145 (2022).
10. Serrano, J.R., Piqueras, P., De la Morena, J., Sanchis, E.J.: Late fuel post-injection influence on the dynamics and efficiency of wall-flow particulate filters regeneration. Appl. Sci. **9**, 5384 (2019).
11. Cherkkil, A., Rathor, A.: Design and optimization of a muffler integrated with an adaptive quarter wave tube for noise reduction in commercial vehicles. SAE Technical Paper 2020-01- 0507 (2020).
12. Jiang, C., Wu, T.W., Xu, M.B., Cheng, C.Y.R.: BEM modeling of mufflers with diesel particulate filters and catalytic converters. Noise Control Eng. J. **58**, 243-250 (2010).
13. Glav, R., Boden, H., Abom, M. An acoustic model for automobile catalytic converters. Proc. Inter-Noise 88, 1261-1266 (1988).
14. Hua, X., Herrin, D.W., Wu, T.W., Elnady, T.: Simulation of diesel particulate filters in large exhaust systems. Appl. Acoust. **74**, 1326-1332 (2013).
15. Torregrosa, A.J., Arnau, F.J., Piqueras, P., Sanchis, E.J., Tartoussi, H.: Phenomenological methodology for assessing the influence of flow conditions on the acoustic response of exhaust aftertreatment systems. J. Sound Vib. **396**, 289-306 (2017).
16. Montenegro, G., Onorati, A., Della Torre, A., Torregrosa, A.J.: The 3Dcell approach for the acoustic modeling of after-treatment devices. SAE Int. J. Engines **4**, 2519-2530 (2011).
17. Allam, S., Abom, M.: Acoustic modelling and testing of diesel particulate filters. J. Sound Vib. **288**, 255-73 (2005).
18. Astley, R.J., Cummings, A.: Wave propagation in catalytic converters: Formulation of the problem and finite element to solution scheme. J. Sound Vib. **188**, 635-657 (1995).
19. Allam, S., Abom, M.: Sound propagation in an array of narrow porous channels with application to diesel particulate filters. J. Sound Vib. **291**, 882-901 (2006).
20. Wenzhi, G., Liming, F., Wenbo, N., Hui, W.: Theoretical and experimental investigations on diesel particulate filters. Noise Control Eng. J. **56**, 282-287 (2008).
21. Ferrara, G., Vichi, G., Lenzi, G., Biliotti, D.: Acoustic characterization of automotive mufflers - Part I: Test rig design and evaluation of acoustic properties. SAE Technical Paper 2012-01-0800 (2012).

22. Drant, J., Micheau, P., Berry, A. Active noise control of higher modes in a duct using near field compensation and a ring of harmonic acoustic pneumatic sources. Appl. Acoust. **188**, 108583 (2022).
23. Abom, M.: Measurement of the scattering-matrix of acoustical 2-ports. Mech Syst. Signal Process. **5**, 89-104 (1991).
24. Chung, J.Y., Blaser, D.A.: Transfer function method of measuring in-duct acoustic properties. II. Experiment. J. Acoust. Soc. Am. **68**, 914-921 (1980).
25. Torregrosa, A.J., Broatch, A., García-Tíscar, J., Roig, F.: Experimental verification of hydrodynamic similarity in hot flows. Exp. Therm. Fluid Sci. **119**, 110220 (2020).
26. Payri, F., Desantes, J.M., Broatch, A.: Modified impulse method for the measurement of the frequency response of acoustic filters to weakly nonlinear transient excitations. J. Acoust. Soc. Am. **107**, 731-8 (2000).
27. Bannister, F.K., Muklow, G.F.: Wave action following sudden release of compressed gas from a cylinder. Proc. Inst. Mech. Eng. **159**, 269-87 (1948).
28. Torregrosa, A.J., Piqueras, P., Sanchis, E.J., Guilain, S., Dubarry, M.: Assessment of acoustic reciprocity and conservativeness in exhaust aftertreatment systems. J. Sound Vib. **436**, 46–62. (2018).
29. Piñero, G., Vergara, L., Desantes, J.M., Broatch, A.: Estimation of velocity fluctuation in internal combustion engine exhaust systems through beam forming techniques. Meas. Sci. Technol. **11**, 1585-95 (2000).
30. Piumetti, M., van der Linden, B., Makkee, M., Miceli, P., Fino, D., Russo, N., Bensaid, S.: Contact dynamics for a solid-solid reaction mediated by gas-phase oxygen: study on the soot oxidation over ceria-based catalysts. Appl. Catal. B **199**, 96-107 (2016).
31. Payri, F., Desantes, J.M., Torregrosa, A.J.: Acoustic boundary condition for unsteady one-dimensional flow calculations. J. Sound Vib. **188**, 85-110 (1995).
32. Morel, T., Silvestri, J., Goerg, K., Jebasinski, R.: Modeling of engine exhaust acoustics. SAE Technical Paper 1999-01-1665 (1999).